

# Models of Random Sparse Eigenmatrices & Bayesian Analysis of Multivariate Structure

Andrew Cron\* & Mike West<sup>†‡</sup>

Original technical report, September 2012. This revised version: September 2014<sup>§</sup>

Final paper published in: *Statistical Analysis for High Dimensional Data*,  
eds: Frigessi *et al*, Abel Symposia 11, Springer International, pp123-154.

## Abstract

We discuss probabilistic models of random covariance structures defined by distributions over sparse eigenmatrices. The decomposition of orthogonal matrices in terms of Givens rotations defines a natural, interpretable framework for defining distributions on sparsity structure of random eigenmatrices. We explore theoretical aspects and implications for conditional independence structures arising in multivariate Gaussian models, and discuss connections with sparse PCA, factor analysis and Gaussian graphical models. Methodology includes model-based exploratory data analysis and Bayesian analysis via reversible jump Markov chain Monte Carlo. A simulation study examines the ability to identify sparse multivariate structures compared to the benchmark graphical modelling approach. Extensions to multivariate normal mixture models with additional measurement errors move into the framework of latent structure analysis of broad practical interest. We explore the implications and utility of the new models with summaries of a detailed applied study of a 20–dimensional breast cancer genomics data set.

*Key Words and Phrases:* Bayesian sparsity models; Givens rotations; Graphical models; Mixtures of sparse factor analyzers; Mixtures of graphical models; Random orthogonal matrix; Sparse eigenmatrices; Sparse variance matrix; Sparse factor analysis; Sparse precision matrix

---

\*84.51° and Duke University. [andrew.j.cron@gmail.com](mailto:andrew.j.cron@gmail.com)

†Duke University. [mw@stat.duke.edu](mailto:mw@stat.duke.edu)

‡Research partly supported by grants from the National Science Foundation [DMS-1106516] and the National Institutes of Health [1RC1-AI086032]. Any opinions, findings and conclusions or recommendations expressed in this work are those of the authors and do not necessarily reflect the views of the NSF or NIH.

§The final publication is available at Springer via [http://dx.doi.org/10.1007/978-3-319-27099-9\\_7](http://dx.doi.org/10.1007/978-3-319-27099-9_7)

# 1. Introduction

We are interested in Bayesian modelling approaches to sparsity in variance and precision matrices in multivariate normal distributions. With interests in parsimony and scalability of analyses of multivariate data in models such as Gaussian mixtures for classification, priors that encourage sparse component covariance patterns are increasingly key as dimension increases. New modelling frameworks also need to enable efficient computational methods for model fitting, which can otherwise be a barrier to application.

Among recent related developments, traditional sparsity priors from model selection in regression have been exploited in sparse extensions of Bayesian factor analysis [36, 2, 39], and in complementary approaches using Gaussian graphical models [20, 8, 30]. The developments in the current work represent natural extensions of the thinking behind these models—building sparsity into variance or precision matrices—while naturally linking and bridging between factor models and graphical models.

The new “sparse Givens” models introduced and developed here arise from new theory of random sparse eigenmatrices; these define eigenstructure of variance and precision matrices, and so induce new classes of priors over Gaussian graphical models. Compared to factor analysis, we avoid the assumption of a reduced dimensional latent factor structure, and the choices it involves. Our new models arise from an inherent theoretical feature of eigenmatrices, rather than hypothesized model structures. We also face fewer challenges in hyper-parameter specification and tuning to fit models. Our models can in fact be viewed as full-rank factor models with sparse, square factor loadings matrices. Additional related work has explored new classes of priors over variance matrices through varying parametrizations, such as partial correlations or Cholesky decompositions [6, 23], that could be extended with sparsity priors. Some such extensions to time series contexts [29, 13] show the utility of various Cholesky-style approaches. Our approach relates to this general literature in that it uses an inherent theoretical property of eigenmatrices that naturally defines the reparametrization as well as an underlying set of parameters that, when set to zero, define parsimonious models.

Section 2 introduces the theoretical and modelling ideas; the approach is based on the Givens rotation representation of full-rank eigenmatrices [1]. We describe how this can be exploited to define new classes of random sparse eigenmatrices, and relate these to decomposable graphical models. Section 3 considers prior specification over variance matrices using this new parametrization, in the context of normal random samples. Section 4 discusses properties of the likelihood and aspects of exploratory data analysis that give insights into sparsity structure of eigenmatrices in our framework, with an example using a 20–dimensional gene expression data set. Section 5 discusses full Bayesian model fitting using a customized reversible jump Markov Chain Monte Carlo approach. We make a detailed, simulation-based comparison with traditional Gaussian graphical modelling (GGM) in 6. Section 7 discusses embedding the basic model into more practicable contexts involving measurement errors and normal mixture models. That section concludes with a detailed example using breast cancer gene expression data, where underlying components relate to known, broad and intersecting cancer subtypes with expected sparsity in dependence, and conditional dependence patterns of subsets of the genes. Section 8 concludes with additional comments and potential extensions.

## 2. Structure and Sparsity in Eigenmatrices

We discuss Givens representations of variance matrices, introduce the general idea of sparsity modelling in this context, and explore aspects of the theoretical structures that emerge under priors over the resulting models.

## 2.1 Givens Rotator Product Representation

Consider a random  $q$ -vector  $\mathbf{x}$  with variance matrix  $\mathbf{V} = \text{Var}(\mathbf{x})$ . The spectral representation (principal component decomposition) is  $\mathbf{V} = \mathbf{RDR}'$  where  $\mathbf{R}$  is the  $q \times q$  orthogonal matrix of eigenvectors– the eigenmatrix– and  $\mathbf{D} = \text{diag}(d_1, \dots, d_q)$  is the matrix of non-negative eigenvalues. The corresponding precision matrix is  $\mathbf{K} = \mathbf{RAR}'$  with  $\mathbf{A} = \mathbf{D}^{-1} = \text{diag}(a_1, \dots, a_q)$ . The general Givens rotator product representation of  $\mathbf{R}$  [1, 38] is

$$\begin{aligned} \mathbf{R} = & \mathbf{O}_{1,2}(\omega_{1,2}) \mathbf{O}_{1,3}(\omega_{1,3}) \dots \mathbf{O}_{1,q}(\omega_{1,q}) \times \\ & \mathbf{O}_{2,3}(\omega_{2,3}) \dots \mathbf{O}_{2,q}(\omega_{2,q}) \times \\ & \vdots \\ & \mathbf{O}_{q-1,q}(\omega_{q-1,q}) \times \mathbf{Q} \end{aligned} \quad (1)$$

where  $\mathbf{Q}$  is diagonal with elements  $\pm 1$ , and each  $\mathbf{O}_{i,j}(\omega_{i,j})$  is a Givens rotation matrix

$$\mathbf{O}_{i,j}(\omega_{i,j}) = \begin{matrix} & & i & & j & & \\ & & & & & & \\ i & \begin{pmatrix} I & 0 & 0 & 0 & 0 \\ 0 & \cos(\omega_{i,j}) & 0 & \sin(\omega_{i,j}) & 0 \\ 0 & 0 & I & 0 & 0 \\ 0 & -\sin(\omega_{i,j}) & 0 & \cos(\omega_{i,j}) & 0 \\ 0 & 0 & 0 & 0 & I \end{pmatrix} & & & & \\ j & & & & & & \\ & & & & & & \end{matrix} \quad (2)$$

for some rotator angles  $\omega_{i,j}$ , ( $i = 1 : q$ ,  $j = i + 1 : q$ ). Some comments and notation follow.

- The angles  $\omega_{i,j}$  lie in  $(-\pi/2, \pi/2]$ . Write  $\boldsymbol{\omega}$  for the set of these  $m = q(q-1)/2$  angles.
- This decomposition of  $\mathbf{R}$  into  $m$  angles is unique and linked to the specific order of the variables in  $\mathbf{x}$ .
- For our goal of covariance modelling, note that  $\mathbf{Q}$  cancels in  $\mathbf{RDR}'$ ; hence,  $\mathbf{Q}$  plays no role and we set  $\mathbf{Q} = \mathbf{I}_q$  with no loss when focused on modelling variance matrices via this decomposition.
- Covariance patterns in  $\mathbf{V}$  can be viewed as successively built-up by pairwise rotations of initial uncorrelated random variables. Take a  $q$ -vector  $\mathbf{e}$  with  $\text{Var}(\mathbf{e}) = \mathbf{D}$ ; then dependencies are defined by successive left multiplication of  $\mathbf{e}$  by the rotator matrices: first by  $\mathbf{O}_{q-1,q}(\omega_{i,j})$ , then  $\mathbf{O}_{q-2,q}(\omega_{i,j})$ , and so on up to  $\mathbf{O}_{1,2}(\omega_{i,j})$  to define  $\mathbf{x} = \mathbf{Re}$  (assuming  $\mathbf{Q} = \mathbf{I}_q$  as noted).
- If  $\omega_{i,j} = 0$  for any  $(i, j)$ , then  $\mathbf{O}_{i,j}(0) = \mathbf{I}_q$  and that rotation has no contribution to the build-up of dependencies and is effectively removed from the representation of equation (1).
- If  $\omega_{i,j} = \pi/2$  for any  $(i, j)$ , then  $\mathbf{O}_{i,j}(\pi/2)\mathbf{MO}'_{i,j}(\pi/2)$  permutes rows  $i$  and  $j$ , and columns  $i$  and  $j$ , of any square matrix  $\mathbf{M}$  and hence does not affect the sparsity of  $\mathbf{M}$ .
- The spectral representations of  $\mathbf{V}$  and  $\mathbf{K}$  are unique only up to permutations of the columns  $\mathbf{R}$ , i.e., reordering of the eigenvalues. Any reordering of the eigenvalues will generate a decomposition as in equation (1) but with different values of the rotator angles. For identification, therefore, we will constrain to  $d_1 > d_2 > \dots > d_q$ . For variance matrices in models of data distributions, the  $d_i$  will be distinct so a strict ordering can be assumed.

## 2.2 Sparse Givens Models

The general representation above reparametrizes  $\mathbf{V}$  to the  $m = q(q-1)/2$  angles in  $\omega$  and the  $q$  eigenvalues in  $\mathbf{D}$ . We note above the role of zero angles, and this opens the path to defining sparse Givens models, i.e., products of fewer than the full set of rotators defining a resulting sparse eigenmatrix: if a large number of the angles are zero, then  $\mathbf{R}$  will become sparse. This can induce a sparse variance matrix  $\mathbf{V}$  and, equivalently, a sparse precision matrix  $\mathbf{K}$  as a result.

Let  $\mathcal{M} = \{(i, j); i = 1 : (q-1), j = (i+1) : q\}$  with  $|\mathcal{M}| = q(q-1)/2 := m$ . Then equation (1) is compactly written as  $\mathbf{R} = \prod_{k=1}^m \mathbf{O}_{m_k}(\omega_{m_k})$  where  $m_k$  is the  $k^{\text{th}}$  pair of dimensions in  $\mathcal{M}$ . Now allow exact zeros in  $\omega$ . Define a sparsity defining index sequence  $\mathcal{S} = \{(i, j) \in \mathcal{M} : \omega_{i,j} = 0\}$  with cardinality  $|\mathcal{S}| = s$ , and set  $\mathcal{Z} = \mathcal{M} \setminus \mathcal{S}$  with size  $z = m - s$ . In words,  $\mathcal{Z}$  is a sequence of  $z \leq m$  ordered pairs  $(i_k, j_k)$  denoting the relevant, non-identity Givens rotation matrices in equation (1) and

$$\mathbf{R} = \prod_{k=1}^z \mathbf{O}_{Z_k}(\omega_{i_k, j_k}). \quad (3)$$

Assuming that priors support exact zeros in  $\omega$ , a primary modelling goal is then to learn  $\mathcal{Z}$  and the corresponding non-zero angles.

Among the features of this approach is that we are able to model full-rank, orthogonal matrices with a parsimonious set of angles, and we maintain the computational convenience of the full-rank spectral parametrization when inverting  $\mathbf{V}$  and  $\mathbf{K}$ . This is especially useful in evaluating density functions in Metropolis Hastings acceptance ratios and, later, in computing normal mixture classification probabilities.

## 2.3 Conditional Independence Graphs

The process of successively building dependencies by adding rotators (from right to left) in equation (3) induces ties between the variables whose variance matrix is the resulting  $\mathbf{V}$ . The resulting structure of  $\mathbf{K} = \mathbf{V}^{-1}$  connects to Gaussian graphical modelling [21, 7, 20, 3, 8, 30].

View the  $q$  variables in  $\mathbf{x}$  as nodes of a graph in which conditional independencies are represented by lack of edges between node pairs. Specifically, this is the undirected graph  $\mathcal{G} = (\mathcal{V}, \mathcal{E})$  with the  $q$  nodes, or vertices, in the vertex set  $\mathcal{V} = \{1 : q\}$ ; two vertices  $(i, j)$  are connected by an edge in the graph if, and only if,  $K_{i,j} \neq 0$  where  $K_{i,j}$  is the  $(i, j)$ -element of  $\mathbf{K}$ . The edge set is  $\mathcal{E} = \{(i, j) : K_{i,j} \neq 0\}$ .

Any precision matrix  $\mathbf{K}_0$  having some off-diagonal zero elements has an implied graph  $\mathcal{G}_0$ . Now take  $\mathbf{K}_1 = \mathbf{O}_{i,j} \mathbf{K}_0 \mathbf{O}'_{i,j}$  where  $\omega_{i,j} \neq 0$  and  $\omega_{i,j} \neq \pi/2$ , with implied graph  $\mathcal{G}_1$ . Notice that left multiplication of  $\mathbf{R}_0$  by  $\mathbf{O}_{i,j}$  simply replaces the  $i^{\text{th}}$  and  $j^{\text{th}}$  rows of with a linear combination of the two. Therefore, the indices of the non-zero elements of the  $i^{\text{th}}$  and  $j^{\text{th}}$  rows of  $\mathbf{R}_1$  are the union of the indices of the  $i^{\text{th}}$  and  $j^{\text{th}}$  rows of  $\mathbf{R}_0$ . Similar comments apply to right multiplication. As a result, the sparsity pattern of  $\mathbf{K}_1$  is the same as that of  $\mathbf{K}_0$  except in rows and columns  $i$  and  $j$ . Specifically, those rows and columns have sparsity indices that are the unions of the those in  $\mathbf{K}_0$ . This shows that the additional rotator  $\mathbf{O}_{i,j}$  maps the graph  $\mathcal{G}_0 = (\mathcal{V}, \mathcal{E}_0)$  to  $\mathcal{G}_1 = (\mathcal{V}, \mathcal{E}_1)$  as follows. With  $\mathcal{N}_j(i) = \{(j, k) : (i, k) \in \mathcal{E}_0\}$ , then  $\mathcal{E}_1 = \mathcal{E}_0 \cup (i, j) \cup \mathcal{N}_i(j) \cup \mathcal{N}_j(i)$ . In words,  $\mathcal{G}_1$  takes  $\mathcal{G}_0$ , connects  $i$  and  $j$ , and unions their neighborhoods.

This structure also generates constructive insights into the nature of the graphical models so defined. It shows that adding a new rotator to an existing sparse Givens model merges the complete subgraphs (cliques) in which the rotators pair  $(i, j)$  reside into one larger clique. Starting at an empty graph, this leads to graphs that are decomposable, formally shown as follows.

**Theorem 1.** *The conditional independence graph  $\mathcal{G}$  implied by a sparse  $\mathbf{K} = \mathbf{R}\mathbf{A}\mathbf{R}'$  under  $\mathcal{Z}$  is a decomposable graph.*

*Proof.* It is enough to show that  $\mathcal{G}$  has a perfect elimination ordering; that is, an ordering of the vertices of the graph such that, for each vertex  $v \in \mathcal{V}$ , the neighbors of  $v$  that occur after  $v$  in the order form a clique [11]. We do this by induction, beginning with no rotations:  $\mathbf{R}_0 = \mathbf{I}_q$  and  $\mathbf{K}_0 = \mathbf{A}$ . This implies that  $\mathcal{G}_0$  is the empty graph and the perfect elimination ordering is trivial. For the inductive step, assume that an ordering exists for the graph implied by a current set of Givens rotations defining  $\mathbf{R}_0$  and  $\mathcal{G}_0$ . Now take  $\mathbf{K}_1 = \mathbf{O}_{i,j} \mathbf{K}_0 \mathbf{O}'_{i,j}$  where  $\omega_{i,j} \neq 0$  and  $\omega_{i,j} \neq \pi/2$ , with implied graph  $\mathcal{G}_1$ . Note that there is no loss of generality here;  $\omega_{i,j} = \pi/2$  would imply simply swapping the  $i$  and  $j$  rows and columns of  $\mathbf{K}_0$  to make  $\mathbf{K}_1$ , and so always yields another decomposable graph. It is now enough to show that  $\mathcal{G}_1$  has a perfect elimination ordering.

Start with the ordering of  $\mathcal{G}$  given by  $\mathcal{U} = \{v_1, v_2, \dots, v_q\} \equiv \{1, 2, \dots, q\}$ . Now take the ordering for  $\mathcal{G}_1$  to be  $\tilde{\mathcal{U}} = \{v_1, \dots, v_{i-1}, \dots, v_{i+1}, \dots, v_{j-1}, v_{j+1}, \dots, v_q, v_i, v_j\}$ . It is enough to show that  $\tilde{\mathcal{U}}$  is a perfect elimination ordering for  $\mathcal{G}_1$ . Take  $v^* \in \tilde{\mathcal{U}}$  and let  $\eta$  be  $v^*$  and its neighbors that occur after  $v^*$  in  $\tilde{\mathcal{U}}$ . We need to show that  $\eta$  forms a clique in  $\mathcal{G}_1$ . If  $v^* = v_1, v_i$ , or  $v_j$ , this is trivial. If  $v^*$  is not a neighbor of either  $v_i$  or  $v_j$  in  $\mathcal{G}_0$ , the rotation has no effect on the neighborhood of  $v^*$  and  $\eta$  is a clique. Now suppose that  $v^*$  is a neighbor of  $v_i$  in  $\mathcal{G}_0$ . Due to our construction of  $\mathcal{G}_1$ , the neighbors of  $v^*$  in  $\mathcal{G}_0$  become neighbors of  $v_i$  in  $\mathcal{G}_1$ . Since  $\eta \setminus v_i$  is a clique in  $\mathcal{G}_0$ , then  $\eta$  will remain a clique in  $\mathcal{G}_1$ . Since  $v_i$  and  $v_j$  were moved to the end of the ordering and  $\eta \setminus v_i$  comes after  $v^*$  in  $\tilde{\mathcal{U}}$  by the inductive hypothesis, then  $\tilde{\mathcal{U}}$  is a perfect elimination ordering of  $\mathcal{G}_1$ .  $\square$

Note that the above concerns general, unrestricted values of the non-zero angles. Furthermore, this applies to any ordering of the rotators where equation (1) is a special case. There are sparse precision matrices whose graphs are decomposable but that do not have a sparse Givens representations for their eigenmatrices. These arise, in particular, in parametric models where the variance and precision matrix are initially defined as functions of lower dimensional parameters to begin; in such cases, the resulting eigenmatrices are inherently structured and typically not sparse, even though the precision matrices are sparse. The simplest example is that of the dependence structure for a set of  $q$  consecutive values of a stationary, linear, Gaussian first-order autoregressive process. There  $\mathbf{K}$  is tri-diagonal, and neither  $\mathbf{R}$  nor  $\mathbf{V}$  is sparse. While  $\mathbf{R}$  has the Givens representation, all  $m$  angles are required and they are deterministically related.

In the next section we define priors for the rotator angles  $\omega$ . This includes conditional priors for the effective angles—excluding values of 0 and  $\pi/2$ —under which these angle are a random sample from a continuous distribution. In such cases, which can be regarded as all practicable cases for applied data analysis, we find a surprising connection between sparse graphical models and sparse factor models; that is, they coincide in this new sparse Givens approach.

**Theorem 2.** *If the angles  $\omega_{i,j} \in \mathcal{Z}$  defining a sparse eigenmatrix are a random sample from a continuous distribution, then the resulting patterns of zeros in  $\mathbf{V}$  and  $\mathbf{K} = \mathbf{V}^{-1}$  are the same with probability one.*

*Proof.* For any  $(i, j)$  pair,

$$V_{i,j} = \sum_{k=1}^q d_k R_{i,k} R_{j,k} \text{ and } K_{i,j} = \sum_{k=1}^q a_k R_{i,k} R_{j,k}.$$

Therefore, zero values of  $V_{i,j}$  and  $K_{i,j}$  follow when

$$\forall k \in \{1, \dots, q\} R_{i,k} = 0 \text{ or } R_{j,k} = 0.$$

However, any other case giving  $V_{i,j} = 0$  requires specific values of  $\mathbf{D}$ , and/or specific relationships among elements of  $\mathbf{V}$  and  $\mathbf{D}$  defining the deterministic constraint that the above sum be zero. Such a constraint will not yield  $K_{i,j} = 0$  under a continuous prior over the angles.  $\square$

### 3. Sparsity Priors on Eigenstructures

We overlay the theoretical framework above with priors that define interesting theoretical models of random variance matrices as well as the specifications necessary for Bayesian analysis.

#### 3.1 Class of Priors

We specify priors that give positive probability to zero values among the angles, allowing row and column flips via angles of  $\pi/2$ , and that otherwise draw angles independently from a continuous distribution. Specifically, the  $m$  angles  $\omega_{i,j}$  are a random sample from a distribution with density

$$p(\omega) = \beta_{\frac{\pi}{2}} I(\omega = \pi/2) + (1 - \beta_{\frac{\pi}{2}}) \beta_0 I(\omega = 0) + (1 - \beta_{\frac{\pi}{2}})(1 - \beta_0) p_c(\omega) \quad (4)$$

where  $I(\cdot)$  is the indicator function and  $p_c(\omega)$  a continuous density on  $(-\pi/2, \pi/2)$ .

Since  $\omega_{i,j} = \pi/2$  does not effect the sparsity of  $R$  and is needed for permuting the effects of the eigenvalues as discussed earlier, we do not want to penalize permutations in the same way as other non-zero angles. We specify the prior in three stages. First with probability  $\beta_{\frac{\pi}{2}}$ ,  $\omega_{i,j} = \pi/2$  to complement the constraint on eigenvalues  $d_i$  being ordered. Then, for angles that do not induce a permutation, we allow zero values with a non-zero conditional probability  $\beta_0$ . Finally, conditional on  $\omega_{i,j} \neq 0$  or  $\pi/2$ , it follows a continuous prior  $p_c(\cdot)$ .

There are various choices of the continuous prior component  $p_c(\cdot)$ . Our examples here use a specific form that seems relevant for use as a routine, namely

$$p_c(\omega) = c(\kappa) \exp \{ \kappa \cos^2(\omega) \} I(|\omega| < \pi/2) \quad (5)$$

where  $\kappa > 0$  and  $c(\kappa)$  is a normalizing constant. In Bayesian analyses via reversible jump MCMC methods we need the value of  $c(\kappa)$  and it can be easily evaluated using any standard numerical integration technique. This prior is unimodal and symmetric about zero, so represents appropriate centering relative to the “null hypothesis” value at zero. The prior concentrates more around zero for larger values of  $\kappa$ , while  $\kappa \rightarrow 0$  leads to the limiting uniform distribution on  $(-\pi/2, \pi/2)$ . The specific mathematical form is also suggested by the forms of conditional likelihood functions for angles in normal models, as noted below in Section 4.

The prior is completed by specifying a distribution for the eigenvalues  $\mathbf{D} = \text{diag}(d_1, d_2, \dots, d_q)$  of  $\mathbf{V}$ . As discussed above, we take them ordered as  $d_1 > d_2 > \dots > d_q$ . The natural, conditionally conjugate class of priors takes the  $d_j$  as ordered values of  $q$  independent draws from an inverse gamma distribution: given some chosen hyperparameters  $(\eta_1, \eta_2)$ , draw  $d_i^{-1} \sim Ga(\eta_1/2, \eta_2/2)$  independently then impose the ordering.

A specified prior over  $(\omega, \mathbf{D})$  leads to the implied prior over  $\mathbf{V}$  and  $\mathbf{K}$ , and within that a prior over the sparsity structure that relates to the random graphical model induced. Simulation of  $p(\omega, \mathbf{D})$  yields simulations from the latter. One aspect of interest is to understand how sparsity in  $\mathbf{R}$  is related to the number of rotators. A follow-on question is how these then relate to sparsity in  $\mathbf{K}$  and hence the sparsity of the implied graph. This is trivially explored by simulation and then simply counting the number of zeros in  $\mathbf{R}$  and  $\mathbf{K}$ . For a given set of rotator pairs  $\mathcal{Z}$  with  $z = |\mathcal{Z}|$ , randomly pick which rotations will be non-zero then sample their angles uniformly and generate  $\mathbf{R}$  and  $\mathbf{K}$ . We repeat this process 10,000 times for each  $0 < z < m$ . For each dimension  $q = 20, 30$ , Figure 1 shows the median proportion of zeros in  $\mathbf{R}$  and  $\mathbf{K}$  as the proportion of non-zero rotators increases. Note how quickly the sparsity of  $\mathbf{K}$ , defining the sparsity of the underlying graph, decreases relative to  $\mathbf{R}$ . This gives some insights into how the choice of the prior sparsity probability  $\beta_0$  plays a role in generating sparse graphs.



where  $\Phi_{i,j} = \mathbf{H}_{i,j} \mathbf{S}_{i,j} \mathbf{H}'_{i,j}$ ,  $\Psi_{i,j} = \mathbf{H}_{i,j} \mathbf{A}_{i,j} \mathbf{H}_{i,j}$  and  $\Gamma_{i,j} = \mathbf{H}_{i,j} \mathbf{A}_{i,j} \mathbf{S}_{i,j} \mathbf{H}'_{i,j} - \Psi_{i,j} \Phi_{i,j}$ . Some specific points to note are as follows:

- The form of the conditional likelihood is the kernel of a matrix Bingham von-Mises Fisher distribution for  $\mathbf{G}(\omega_{i,j})$  [17], which suggests such distributions as conditionally conjugate priors.
- As a function of the scalar angle  $\omega_{i,j}$ , it is trivially shown that the log likelihood is a quadratic form in  $(\sin(\omega_{i,j}), \cos(\omega_{i,j}))$ . It is easy to numerically maximize this conditional log likelihood. As a result, iterative maximum likelihood estimates can be derived by sequentially maximizing the above conditional likelihood functions as we iterate over rotators  $(i, j)$ , coupled with conditional maximization over the eigenvalues.
- In the special case of  $\mathbf{R}_{i,j,1} = \mathbf{I}_q$ , i.e., when  $(i, j)$  is the right-most rotator pair and  $\mathbf{A}_{i,j} = \mathbf{A}$ , the conditional likelihood can be maximized analytically if the diagonal of  $\mathbf{A}$  is not constrained to be ordered. The maximizing  $\omega_{i,j}$  value satisfies  $\tan(2\hat{\omega}_{i,j}) = 2s_{i,j}/(s_{j,j} - s_{i,i})$  where  $s_{a,b}$  are the scalar entries of the “decorrelated” sample variance matrix  $\mathbf{S}_{i,j}$ . Given this value, including  $\mathbf{A}$  in the conditional log likelihood maximization gives the following:

$$\begin{aligned}\hat{\omega}_{i,j} &= \frac{1}{2} \arctan \left( \frac{2s_{i,j}}{s_{j,j} - s_{i,i}} \right), \\ n\hat{a}_i^{-1} &= s_{i,i} \cos^2(\hat{\omega}_{i,j}) + s_{j,j} \sin^2(\hat{\omega}_{i,j}) + 2s_{i,j} \cos(\hat{\omega}_{i,j}) \sin(\hat{\omega}_{i,j}), \\ n\hat{a}_j^{-1} &= s_{j,j} \cos^2(\hat{\omega}_{i,j}) + s_{i,i} \sin^2(\hat{\omega}_{i,j}) - 2s_{i,j} \cos(\hat{\omega}_{i,j}) \sin(\hat{\omega}_{i,j}), \\ n\hat{a}_k^{-1} &= s_{k,k} \text{ for } k \neq i, j.\end{aligned}\tag{9}$$

- Continuing in the above case, if all correlation between variables  $i$  and  $j$  has been rotated away by the application of the preceding rotators so that  $s_{i,j} = 0$ , then the conditional MLE of  $\omega_{i,j}$  is zero. In this case, it can also be shown that the conditional likelihood function in  $\omega_{i,j}$  is proportional to  $\cos^2(\omega_{i,j})$ .
- The above confirms the role of a continuous prior  $p_c(\cdot)$ , as in equation (5), as a conditionally conjugate prior centered around the region of no residual correlation between the two variables.

## 4.2 An Exploratory Analysis Algorithm

The investigations of likelihood structure above suggests a simple exploratory analysis that can be of use in generating insights into potential sparsity structure as well as, particularly, defining starting values for a full Bayesian MCMC-based analysis of the sparse eigenmatrix model. This is discussed here in the case of  $\kappa = 0$  in the prior, for simplicity, although could be trivially modified.

Begin with  $\mathbf{S}_* = \mathbf{S}$  and  $\mathbf{R}_* = \mathbf{I}_q$  defining the “current” versions of the decorrelated sample variance matrix and corresponding candidate eigenmatrix, respectively.

1. Set variable index  $i = 1$  and  $j = 2$ .
2. Compute the sample correlation  $r_{i,j}$  from  $\mathbf{S}_*$ .
3. If  $|r_{i,j}|$  is large enough based on some pre-specified threshold which can be linked to the log likelihood difference it implies, add a rotator on pair  $(i, j)$  with angle  $\hat{\omega}_{i,j}$  from equation (9).
4. If the choice is to include a new rotator, update  $\mathbf{R}_*$  to  $\mathbf{R}_* \mathbf{O}(\hat{\omega}_{i,j})$  and further decorrelate the sample variance matrix by updating  $\mathbf{S}_*$  to  $\mathbf{O}(\hat{\omega}_{i,j})' \mathbf{S}_* \mathbf{O}(\hat{\omega}_{i,j})$ .

5. Sequence through the remaining  $(i, j)$  in the order of the rotations in equation (1). Finally, set  $A_*$  to be the MLE based on the decorrelated  $S_*$ .

This forward selection process successively adds optimized rotators via right multiplication, building up the corresponding sequence of pairs of variable indices  $(i, j)$  to define an empirical set  $\mathcal{Z}$  of included rotators. It delivers this empirical estimate of  $\mathcal{Z}$  and the corresponding, optimized estimate of  $\mathbf{R}$ , and hence of  $\mathbf{V}$  and  $\mathbf{K}$  based on a final re-maximization of the likelihood for  $\mathbf{A}$  given the optimized  $\mathbf{R}$ . There are many rules that can be used for the thresholding in step 3. For instance, we could use the absolute value of the conditional MLE,  $\hat{\omega}_{i,j}$ . However, the effect of the rotation on the likelihood is unclear as it depends on the eigenvalues which makes a particular threshold hard to interpret. Simple thresholding on the current, “residual” sample correlation  $|r_{i,j}|$  is natural and interpretable; the squared correlation is the degree of residual structure in  $S_*$  that will be removed in that iteration of the exploratory algorithm. Hence a natural approach is to add a new rotator so long as  $|r_{i,j}| > \rho$  for some specified threshold  $\rho$ .

We note that this fast exploratory algorithm cannot constrain the diagonal of our estimate  $A_*$  to be ordered. For exploration purposes, this is not an issue as the resulting estimate of  $\mathbf{V}$  and  $\mathbf{K}$  will not be affected. Furthermore if we denote by  $A_*$  an exploratory estimate, and let  $\mathbf{P}$  be the permutation matrix such that  $\mathbf{A} = \mathbf{P}A_*\mathbf{P}'$  where the diagonal of  $\mathbf{A}$  is ordered, then  $\mathbf{V} = \mathbf{R}\mathbf{A}\mathbf{R}'$  where  $\mathbf{R} = \mathbf{R}_*\mathbf{P}$ . In words, we are simply finding a sparse spectral decomposition that has the interpretation of a forward selection process based on residual correlation. We then order the eigenvalues and their corresponding eigenvectors. Generating MCMC starting values for  $\omega$  is now simply a matter of finding the unique  $\omega$  that represents  $\mathbf{R}$  in the general Givens rotator product representation. [1] recursively derive  $\omega$  exactly from  $\mathbf{R}$ . Just as many zero elements in  $\omega$  induce zeros in  $\mathbf{R}$ , the starting value for  $\omega$  based on the decomposition of the sparse  $\mathbf{R}$  will have many elements set to zero making this a very fast and effective method for finding sparse starting values.

In supporting material, we provide code implementing this overall algorithm for interested readers.

### 4.3 A Breast Cancer Genomics Example

We consider a subset of the microarray-based gene expression data that is analyzed in more detail in Section 7 below. The subset of size  $n = 66$  represents tumors that would be regarded as aggressive in term of their expression profiles, based on higher levels of expression of genes related to the two key hormonal pathway: the ER (estrogen receptor) and Her2 growth factor pathways [37, 18]. Activity of genes in these two primary, distinct pathways, and their interactions with multiple other biological pathways in cell growth and development, play into our understanding of the heterogeneity of breast cancer, and critically into advances in understanding clinically relevant cancer subtypes [33, 2, 27]. Several of the  $q = 20$  genes, notably the leading 6 in Figure 2 (CA12, GATA3, HNF-3 $\alpha$ , LIV-1, Annexin, TFF3), are in part co-regulated in the ER network, some being directly transcribed by ER along with other factors. These genes vary across this subset of samples and are at relatively high levels of expression. These genes, as well as other breast cancer biomarker genes (C-MYB, BCL-2) that also interact with the ER network, play roles in multiple biological pathways; as a result, their inter-relationships in expression are more complicated than a simple one-dimensional ER factor would explain. Three of the variables (ERB-B2, HER2a, HER2b) are highly related read-outs of activity of the hormonal Her2 pathway (the first two are in fact different sequences from the same primary Her2 gene); other genes in the sample (GRB7, CAB1) are known to be regulated or co-regulated with Her2. Two additional gene sequences (BRCA1, BRCA2) relate to inherent susceptibility to breast cancer; their transcriptional relationships with ER and Her2 are poorly understood, although higher levels tend to be related to low ER and HER1 activity. To give a sense of robustness, 5 additional variables are included: the Junk genes represent random Gaussian noise.

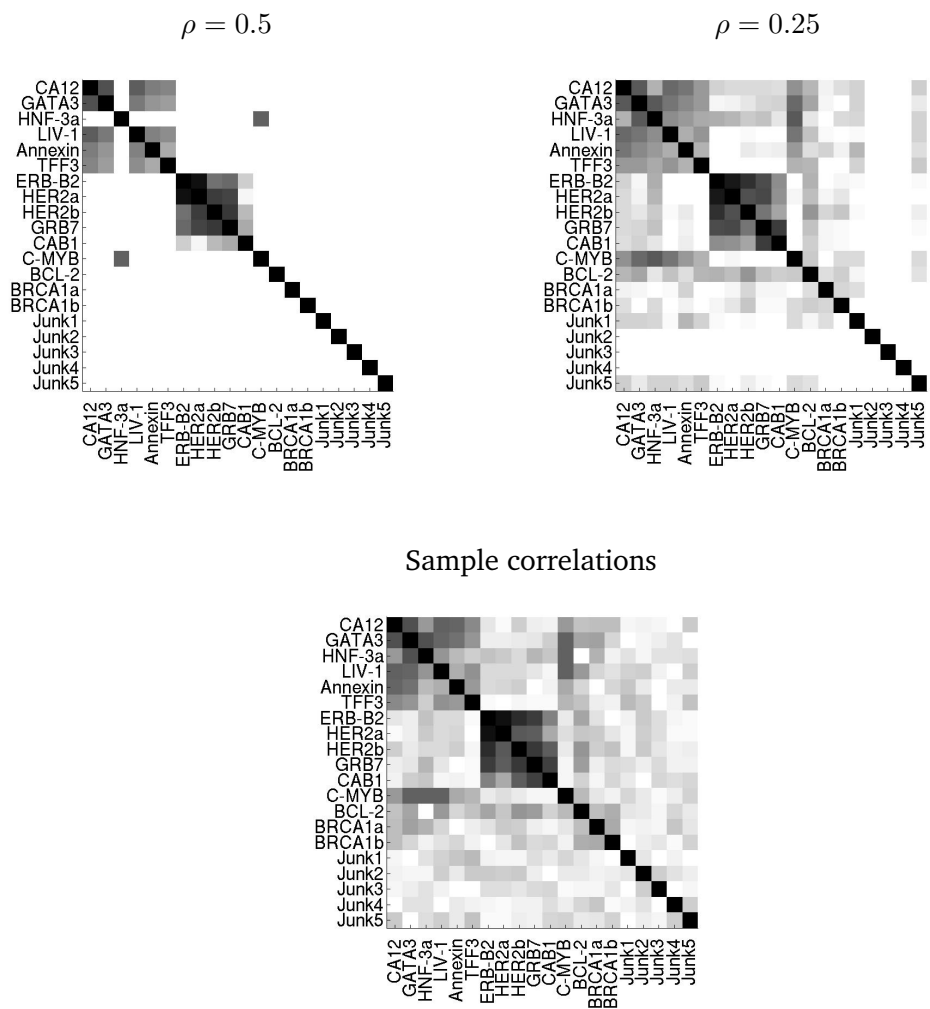


Figure 2: Breast cancer gene expression data example in Section 4.2. Grey-scale heat maps show absolute values of elements in the estimated correlation matrix using the exploratory algorithm (white= 0 correlation, black= 1). The first two frames correspond to stopping the algorithm when the maximum absolute value of the residual correlation drops below  $\rho = 0.5$  compared to  $\rho = 0.25$ , respectively. The third frame shows the full sample correlation matrix.

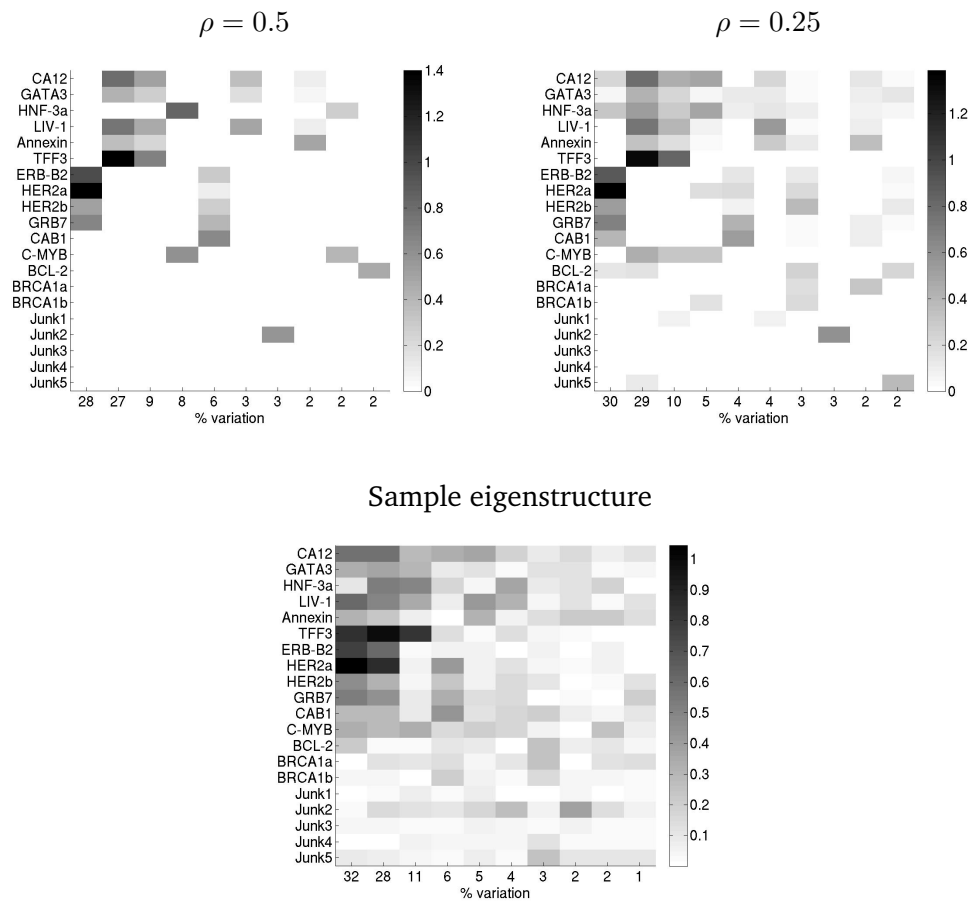


Figure 3: Breast cancer gene expression data example in Section 4.2. Grey-scale heat maps show absolute values of elements in the first ten columns of the estimated scaled eigenmatrix  $RD^{1/2}$  corresponding to the correlation matrix in Figure 2. The x-axes show the percent variation explained by each eigenvector (column) as implied by the empirical estimates of the  $d_j$  in each case.

After centering each of the  $q = 20$  variables, the exploratory analysis was applied twice for a comparison of choice of stopping rule: we used thresholds of  $|r_{i,j}| \geq 0.5$  and  $|r_{i,j}| \geq 0.25$ . A third analysis simply computes the sample correlation matrix and the corresponding eigenmatrix. Graphical summaries of the final estimates of the correlation matrix and the corresponding scaled eigenmatrix appear in Figures 2 and 3, respectively. We can see the increase in sparsity in moving from no thresholding (the sample eigenmatrix) to a threshold of 0.25 and then 0.5, and how the sparse Givens construction—via this simple exploratory estimation method—naturally denoises the raw sample estimates. The major ER and Her2 “clusters” evident in the correlation matrices are sustained as we move up through the levels of thresholding, and the corresponding “factor loadings” structure represented in the eigenmatrices successively reduces the numbers and patterns of genes related to each factor (column). The most sparse structure in the first row shows that—assuming this level of sparsity—we uncover a dominant Her2 factor loaded on four of the Her2 cluster of genes, two main ER factors, and a few minor factors that each represent only modest levels of variation explained while contributing to the break-down of the complexity of expression relationships in the data.

## 5. Bayesian Analysis and Computation

We discuss and develop Bayesian computation for model fitting and exploration, presenting customized MCMC methods.

### 5.1 Overview

In target applications with modest and increasingly high values of  $q$ , and hence larger  $m = q(q - 1)/2$ , the focus is on sparse structures so that posterior distributions will concentrate on smaller numbers of non-zero angles. In these circumstances, visiting every element of  $\omega$  using a Gibbs sampling approach will be computationally expensive and other MCMC strategies are recommended. Most effective MCMC analysis can be achieved using reversible jump Markov Chain Monte Carlo (RJ-MCMC) [12]. We have implemented such an approach based on exploring the space of non-zero elements of  $\omega$  using a birth/death RJ-MCMC. Each move through this “model space” involves proposed changes that introduce non-zero values, including the possible values  $\omega = \pi/2$ , and/or setting current non-zero values to zero. We present the details of the sampling algorithm by first outlining an approximation to the conditional posterior of a single, non-zero  $\omega_{i,j}$  that we recommend as conditional proposal distribution for the MCMC.

### 5.2 Wrapped Cauchy Proposals

Consider any rotator pair  $(i, j)$  assuming  $\omega_{i,j} \neq 0$ . The conditional posterior is proportional to the conditional mixture prior, mixing a point mass at  $\pi/2$  with  $p_c(\cdot)$ , multiplied by the conditional likelihood of the form discussed in the previous section—the conditional likelihood for  $\omega_{i,j}$  given all other rotators and eigenvalues. Our MCMC adopts a conditional proposal distribution for  $\omega_{i,j}$  based on direct approximation. Specifically, we use a proposal with pdf

$$g(\omega) \equiv \beta_{\frac{\pi}{2}} I(\omega = \pi/2) + (1 - \beta_{\frac{\pi}{2}}) g_c(\omega)$$

where the continuous density  $g_c(\cdot)$  is that of a wrapped Cauchy chosen to approximate the conditional posterior for  $\omega_{i,j}$  conditional on  $0 < |\omega_{i,j}| < \pi/2$ ; i.e., a Cauchy “wrapped” onto the interval  $(-\pi/2, \pi/2)$  [10]. Specifically,

$$g_c(\omega) = \frac{1}{\pi} \frac{\sinh(2\sigma)}{\{\cosh(2\sigma) - \cos[2(x - \theta)]\}}$$

where  $(\theta, \sigma)$  are chosen so that  $g(\cdot)$  approximates the conditional posterior under prior  $p_c(\cdot)$ . The proposed values of  $(\theta, \sigma)$  are based on direct numerical approximation. We set  $\theta$  as the exact conditional posterior mode; this is easily evaluated numerically. Under any conjugate prior over non-zero values, which includes our recommended default prior  $p_c(\cdot)$  in (5), note that  $\log p(\omega_{i,j}|\mathbf{X}, -)$  is a quadratic form in  $(\sin(\omega_{i,j}), \cos(\omega_{i,j}))$  on a bounded domain and can be evaluated along with any number of derivatives very quickly. Resulting numerical maximization is then routine and extremely efficient. At the solution  $\theta$ , the curvature generates a value for the scale  $\sigma$  from

$$\frac{1}{\sigma^2} = - \left. \frac{\partial^2}{\partial \omega_{i,j}} \log p(\omega_{i,j}|\mathbf{X}, -) \right|_{\omega_{i,j}=\theta}.$$

The wrapped Cauchy form can be viewed as a diffuse posterior approximation– the result of an initial Laplace approximation subject to inflating the tails to ensure good coverage of the exact conditional posterior. To deal with cases in which the mode  $\theta$  lies on the boundary, simply replacing  $g_c(\cdot)$  with a  $\text{Be}(\omega|0.25, 0.25)$  density has been empirically found to provides an effective, default proposal.

### 5.3 Reversible Jump MCMC

Denote all parameters of interest by  $\Theta = \{\mathcal{Z}, \omega, \mathbf{A}\}$  where, as introduced above,  $\mathcal{Z}$  is the set of pairs of indices  $(i, j)$  corresponding to included rotators with non-zero angles. In an overall MCMC, suppose we are at a current state at iterate  $t$  with parameters  $\Theta^{(t)} = \{\mathcal{Z}^{(t)}, \omega^{(t)}, \mathbf{A}^{(t)}\}$  with a current  $z^{(t)} = |\mathcal{Z}^{(t)}|$  rotators. Consider now either adding or removing a rotator index pair from  $\mathcal{Z}^{(t)}$ . Set probabilities of adding a rotator (birth) and removing a rotator (death) at values denoted by  $p_B$  and  $p_D$ , respectively. For a proposed birth, randomly select an ordered pair,  $(i^*, j^*) \in \mathcal{M} \setminus \mathcal{Z}^{(t)}$  to index a proposed angle, and then generate a proposal  $\omega_{i^*, j^*}^*$  from  $g(\omega_{i^*, j^*}^*)$  described in the Section 5.2. This implies the following birth step accept/rejection ratio:

$$\alpha_B = \frac{p(\mathbf{X}|\omega_{i^*, j^*}^*, -)p(\omega_{i^*, j^*}^*)(z^{(t)} + 1)p_D}{p(\mathbf{X}|\omega_{i^*, j^*}^{(t)}, -)p(0)g(\omega_{i^*, j^*}^*)(m - z^{(t)})p_B}. \quad (10)$$

For a proposed death step, choose an element from  $\mathcal{Z}^{(t)}$  uniformly and set its corresponding angle to zero. The resulting rejection ratio is simply  $\alpha_D = \alpha_B^{-1}$ . We then set  $\omega_{i^*, j^*}^{(t+1)} = \omega_{i^*, j^*}^*$  with probability  $\min(1, \alpha_B)$ . To facilitate better mixing, we do several reversible jump proposals in each MCMC iteration. This results in the updated (possibly, of course, also the same) set of rotator pairs  $\mathcal{Z}^{(t+1)}$ .

The MCMC next updates all non-zero angles indexed in  $\mathcal{Z}^{(t+1)}$ . For each pair  $(i, j) \in \mathcal{Z}^{(t+1)}$ , generate a proposal  $\omega_{i,j}^*$  from  $g(\omega_{i,j})$  and set  $\omega_{i,j}^{(t+1)} = \omega_{i,j}^*$  with probability

$$\min \left\{ 1, \frac{p(\mathbf{X}|\omega_{i,j}^*, -)p(\omega_{i,j}^*)g(\omega_{i,j}^{(t)})}{p(\mathbf{X}|\omega_{i,j}^{(t)}, -)p(\omega_{i,j}^{(t)})g(\omega_{i,j}^*)} \right\}. \quad (11)$$

Since we update the elements of  $\omega^{(t)}$  in order, the recursive relationship between the conditional log likelihoods given in equation (8) makes computation extremely fast. This recursive update is initialized at

$$\mathbf{A}_{i_1, j_1} = \mathbf{O}_{i_1, j_1}(\omega_{i_1, j_1}^{(t)})' \mathbf{R}^{(t)} \mathbf{O}_{i_1, j_1}(\omega_{i_1, j_1}^{(t)}) \quad \text{and} \quad \mathbf{S}_{i_1, j_1} = \mathbf{S}.$$

The log likelihood can then be optimized and evaluated quickly as described in the previous section. For  $k > 1$  as we step through updates of rotator  $k$ , compute

$$\begin{aligned} \mathbf{A}_{i_k, j_k} &= \mathbf{O}_{i_k, j_k}(\omega_{i_k, j_k}^{(t)})' \mathbf{A}_{i_{k-1}, j_{k-1}} \mathbf{O}_{i_k, j_k}(\omega_{i_k, j_k}^{(t)}) \quad \text{and} \\ \mathbf{S}_{i_k, j_k} &= \mathbf{O}_{i_{k-1}, j_{k-1}}(\omega_{i_{k-1}, j_{k-1}}^{(t+1)})' \mathbf{S}_{i_{k-1}, j_{k-1}} \mathbf{O}_{i_{k-1}, j_{k-1}}(\omega_{i_{k-1}, j_{k-1}}^{(t+1)}). \end{aligned}$$

Note that the recursions for  $\mathbf{A}_{i_k, j_k}$  and  $\mathbf{S}_{i_k, j_k}$  only involve taking linear combinations of two rows and columns, so we can avoid recomputing the entire eigenmatrix for every proposal. In words: (i) start with the sum of squares matrix and the eigenmatrix; (ii) remove the first rotation by multiplying by its transpose; (iii) perform a fast Metropolis move by exploiting the quadratic form of the likelihood; (iv) decorrelate the sum of squares matrix with the new rotator and remove the next rotation from the eigenmatrix.

The final step is to update the entries of the diagonal precision matrix  $\mathbf{A}$  from the current value  $\mathbf{A}^{(t)}$ . Let

$$\mathbf{B} = \mathbf{R}^{(t)'} \mathbf{S} \mathbf{R}^{(t)}.$$

Then for each  $j = 1, \dots, q$

$$p(a_j^{(t)} | \mathbf{X}, -) \propto \text{Ga}(a_j^{(t)} | (\eta_1 + n)/2, (\eta_2 + B_{j,j})/2) I(a_{j-1}^{(t)} < a_j^{(t)} < a_{j+1}^{(t)}) \quad (12)$$

where  $Ga(x|a, b)$  denotes the pdf of the  $Ga(a, b)$  distribution evaluated at  $x$ . Since the eigenvalues are constrained to be ordered, the conditional distributions are constrained as well. The resulting constrained gamma distribution is sampled using the inverse cdf method.

## 6. Simulation Study and Comparisons

We make a detailed, simulation-based comparison of the modelling approach with analysis using traditional Gaussian graphical modelling (GGM) [21, 7, 20, 3, 8, 30]. The GGM framework with decomposable graphs is directly comparable and stands as a current benchmark model context.

The simulation study was conducted using zero mean normal models in each of  $p \in \{10, 20, 30, 40, 50, 75, 100\}$  dimensions, with a fixed sample size of  $n = 150$  observations. Synthetic data sets generated from specific model classes were analyzed using the sparse Givens approach and the GGM approach, the latter using shotgun stochastic model search for the Bayesian analysis [20]. Each analysis was repeated for 100 simulation samples. The underlying models and synthetic data generation proceeded as follows:

1. Generate a target precision matrix  $\mathbf{K} = \mathbf{U}'\mathbf{U}$  where  $\mathbf{U}$  is upper triangular with:
  - $\mathbf{U}_{i,i} = \sqrt{\nu_i}$  with  $\nu_i \sim \chi_{p-i}^2$ , ( $i = 1, \dots, p$ ),
  - $\mathbf{U}_{i,j} = u_{i,j} I(|u_{i,j}| > 1)$  where  $u_{i,j} \sim N(0, 1)$ , ( $j > i$ ,  $i = 2, \dots, p-1$ ), and
  - the  $\nu_i, u_{i,j}$  are mutually independent.
2. Draw  $n = 150$  observations  $\mathbf{X}$  as a random sample from  $N(0, \mathbf{K}^{-1})$ .
3. Fit the sparse Givens model using 15,000 MCMC iterations. Discard the first 10,000 and save the final 5,000 as a Monte Carlo sample for sparsity patterns and values of  $\mathbf{K}$ .
4. Fit the GGM model using 15,000 stochastic search iterations. Discard the first 10,000 and save the final 5,000 graphs identified, their posterior probabilities and the parameters of the corresponding posteriors for  $\mathbf{K}$  on each graph.

For prior distributions, the probability of including a “free” parameter was set to  $2/(p-1)$ . In the sparse Givens models, a free parameter is an angle; in GGMs, it is the probability of including a random edge. This specification aims to match the prior expectations of degrees of sparsity between the two approaches.

Comparisons are based on measuring agreement between the approximate posteriors and the “true” underlying data-generating distribution. For any precision matrix  $\mathbf{K}_*$ , we can directly compute the

Kullback-Leibler (KL) divergence of the  $N(0, \mathbf{K}_*^{-1})$  distribution from the true, underlying  $N(0, \mathbf{K}^{-1})$  distribution. With both the MCMC posterior samples and the GGM search results, we can then approximately evaluate the posterior distribution for the KL divergence of the chosen model from the truth.

Figure 4 summarizes the posteriors for the KL divergences, aggregated across 100 repeat samples. We can see that in 20 dimensions, both methods perform similarly; this is not surprising since there is reasonable amount of data relative to the dimension. However, in 30 dimensions, the new sparse Givens approach is significantly better, and its dominance is progressively more pronounced as the dimension increases.

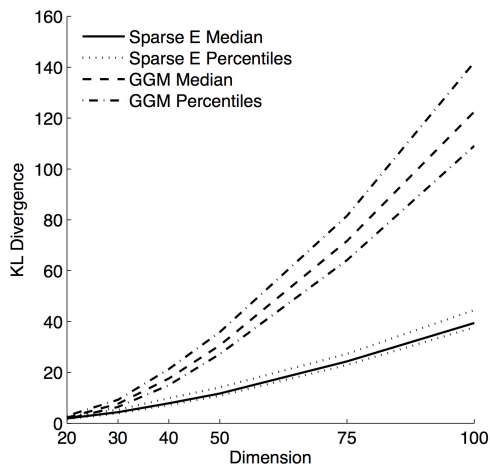


Figure 4: Simulation study comparing GGM to the sparse Givens (labelled “Sparse E” in the figure) methodology. Shown are the medial, 10th and 90th percentiles of the posterior for (logged values of) the KL divergence from the fitted model to the true underlying data generating model.

## 7. Mixtures of Sparse, Full-Rank Factor Models

Many applied contexts involve evident non-Gaussian structure as well as measurement error overlaid on the underlying dependency patterns we are interested in inferring via the sparse eigenmatrix models. The gene expression example of Section 4.2 is just one case-in-point. First, in the broader contexts of samples from the full breast cancer population, there is inherent non-Gaussianity representing heterogeneity in cancer states. This heterogeneity can be regarded as arising from a mixture of sub-populations, or “subtypes” that, in terms of expression data outcomes, are hugely overlapping [33, 2, 27]. More broadly, use of discrete mixtures of Gaussians is a well-established strategy for modelling what might be quite non-Gaussian distributional forms, whether or not there is an inherent in mixture components and discrimination/classification [9, 4, 35]. Second, measurement errors are ubiquitous. Again the gene expression example and broader context is a good example, as the experimental and data extraction contexts are well-known to overlay underlying biological variation with meaningful uncertainties that must be accommodated within a more general model in order to avoid obscuring relationships and leading to potential biases in resulting inferences [26, 2, 24, 25].

## 7.1 Mixture Models and Extension of MCMC Analysis

We address the above, general considerations with Gaussian mixture models overlaid with measurement errors. Each mixture component has a variance matrix modelled via the sparse Givens strategy; this can be directly interpreted as a sparse, full-rank latent factor model for underlying “structural” dependencies. As a result, the overall framework is a generalized, adaptively sparse model for “mixtures of (full-rank, sparse) factor analyzers” [28, 30].

Assume we observe  $n$  independent  $q$ -vector observations  $\mathbf{Y} = \{\mathbf{y}_1, \dots, \mathbf{y}_n\}$  where  $\mathbf{y}_i = \mathbf{x}_i + \boldsymbol{\epsilon}_i$  with independent measurement errors  $\boldsymbol{\epsilon}_i \sim N(\mathbf{0}, \boldsymbol{\Psi})$  having variance matrix  $\boldsymbol{\Psi} = \text{diag}(\psi_1, \dots, \psi_q)$ . Suppose the latent signals  $\mathbf{x}_i$  are independently drawn from a discrete mixture of multivariate normals having pdf

$$p(\mathbf{x}) = \sum_{c=1}^C w_c N(\mathbf{x} | \boldsymbol{\mu}_c, \boldsymbol{\Sigma}_c).$$

Equivalently,

$$\mathbf{y}_i | \gamma_i \sim N(\boldsymbol{\mu}_c, \boldsymbol{\Sigma}_c + \boldsymbol{\Psi}), \quad \text{where} \quad Pr(\gamma_i = c) = w_c,$$

involving the underlying latent mixture component indicators  $\gamma_i$  that are independently drawn from the multinomial distribution on cells  $\{1 : C\}$  with the vector of cell probabilities  $\mathbf{w} = (w_1, \dots, w_C)'$ .

We develop this mixture model under sparse Givens factor structures for each of the mixture components. That is,  $\boldsymbol{\Sigma}_c = \mathbf{R}_c \mathbf{D}_c \mathbf{R}_c'$  where we model each of the  $(\mathbf{R}_c, \mathbf{D}_c)$  with the prior structure of Section 3, independently across components  $c$ . This allows for differing degrees and patterns of sparsity as we move across components of the mixture, in the context of also accommodating realistic assessment of overlaid measurement errors. We couple this with conditionally conjugate normal priors for the  $(\boldsymbol{\mu}_c | \boldsymbol{\Sigma}_c)$  independently across components, and a similarly conditionally conjugate Dirichlet prior for the mixture weights  $\mathbf{w}$ . The final component of prior specification is a set of  $q$  conditionally independent inverse gamma priors for the measurement error variances  $\psi_j, j = 1 : q$ .

The traditional MCMC analysis of multivariate normal mixtures [22, 5] is easily extended to apply here. Several points require note. At each iterate conditional on currently imputed values of the  $\mathbf{x}_i$ , we resample new values of the mixture component indicators  $\gamma_i$  for each of the  $i = 1 : n$  observations. Conditional on these indicators, the imputed signal “data” vectors  $\mathbf{x}_i$  are organized into  $C$  conditionally independent normal subgroups. The inherent component labelling issue is automatically addressed each iteration using the efficient component relabelling strategy of [5]. The numbers of observations in each group define the conditional multinomial sample needed to draw new values of the mixture weights  $\mathbf{w}$  from the implied conditional Dirichlet posterior. We then resample new group means  $\boldsymbol{\mu}_c$  from the implied set of  $C$  conditional normal posteriors. Subtracting the group means from the values of the  $\mathbf{x}_i$  within each group, we are then in a context of having  $C$  replicates of the normal, sparse Givens model. Hence we apply  $C$  parallel RJ-MCMC steps to draw new values of rotator index sets, angles and eigenvalues in each of the components. The final, additional component of the overall MCMC posterior simulation arises due to the additive measurement error structure of the model. Given the resampled parameters and component indicators, the implied conditional posterior for each  $\mathbf{x}_i$  is normal, so easily sampled; given the new value of  $\mathbf{x}_i$ , we compute new synthetic residuals  $\boldsymbol{\epsilon}_i = \mathbf{y}_i - \mathbf{x}_i$  that lead to a set of  $q$ , independent conditional posteriors for the  $\psi_i$  that are each of inverse gamma form.

Additional technical details of these steps appear in the Appendix, and in supporting material, we provide code implementing this MCMC algorithm.

## 7.2 A Broader Study in Breast Cancer Genomics

We analyse a set of  $n = 295$  breast cancer gene expression sample that represent the full range of breast cancers; the data set uses the same 15 genes as in the example of Section 4.2, but now reflecting full population heterogeneity; variations in the expression levels of these 15 breast cancer related genes is much greater across this full set of 295 tumor samples. The  $q = 20$ -dimensional data set again includes 5 “Junk” genes generated as Gaussian noise, to add dimension for the evaluation of the model analysis.

As discussed in Section 4.2, breast cancer heterogeneity based on molecular markers related to ER and Her2 pathways is often regarded in terms of over-lapping cancer subtypes. The genes selected for this study relate to these pathways, and the variability across samples is certainly empirically consistent with at least three underlying components; see some scatter plots on a few genes in Figure 5. We fit the sparse Givens, finite mixture model  $C = 4$ . Priors for residual measurement error variances are informed by a wealth of prior information from studies of gene expression data using Affymetrix microarrays in breast cancer and other contexts [32, 31, 2, 26, 24, 27, 25]. Specifically, we adopt  $\psi_j \sim \text{InvGa}(3.1, 0.17)$  with implied 95% prior credible intervals for measurement error standard deviations of about  $(0.15, 0.5)$ . For the mixture weights  $w$ , we take a uniform Dirichlet prior. For component locations, we take  $\mu_c | \Sigma_c \sim N(\mathbf{0}, \tau \Sigma_c)$  where  $\tau$  is large to induce a rather diffuse marginal prior on mixture locations; the analysis summarized below has  $\tau = 1,000$ . The prior over the sparse Givens parameters for each  $\Sigma_c$  takes  $\beta_0 = 0.99$ ,  $\beta_{\pi/2} = 0.25$ , and  $\kappa = 0$ . This prior expresses an expectation of a fair degree of sparsity in each  $\mathbf{R}_c$ , coupled with a vague uniform prior on values of non-zero angles. Finally for  $\mathbf{D}_c$ , we have  $\eta_1 = 1/1,000$  and  $\eta_2 = 1/1,000$  representing an uninformative prior on the eigenvalues, up to the constraints imposed by their ordering.

For starting values, we first crudely partition the data using  $k$ -means clustering, then use the exploratory algorithm of Section 4.2 with a correlation threshold of 0.5. We run the MCMC for 200,000 iterations, discarding the first 100,000 for burn-in to ensure convergence, with a number of subjective assessments of this. The analysis identifies 3 main components with posterior means of components weights of  $(0.564, 0.303, 0.125, 0.008)'$ . Figure 5 shows some aspects of the posterior through scatter plots of data on a few selected genes. From the MCMC we compute estimates of the sample component classification probabilities  $Pr(\gamma_i = c | \mathbf{Y})$  for each  $i = 1 : n$ , and allocate sample  $i$  to the most probable component for the purpose of this graphical display; the data points are plotted as symbols corresponding to their most probable component. The dominant identified component  $c = 1$  represents cases with expression varying across high levels for genes linked to the ER pathway, including TFF3, CA-12 and GATA3 shown in Figure 5, and with Her2 pathway genes varying at relatively low levels; these represent the broad luminal subtype of breast cancers [33, 2, 27]. The second main component  $c = 2$  represents cases generally high in Her2 expression levels, with other genes varying across the spectrum; this corresponds to high-risk Her2 breast cancers that are generally targets for the Her2 receptor inhibiting drug herceptin. The third, smaller component  $c = 3$  represent the so-called triple-negative/basal-like tumors, with generally low levels of activity of both ER and Her2 related genes. The patterns in the figure, and in those of other genes in the example, as well as the posterior estimates of relative sizes of these three main components, are quite consistent with the known cancer biology and relative probabilities of these three broad, and imprecisely defined clinical subtypes of tumors.

Table 1 summarizes the posterior for the number of non-zero angles in each mixture component and the sparsity of  $\mathbf{R}_c$ . The maximum number of rotators is 105 and the maximum sparsity of  $\mathbf{R}$  is 210. The posterior favours a very sparse set of angles in each mixture component and the eigenstructure in each component is quite sparse as a result.

Figures 6 and 7 give graphical summaries generating insights into the inferred sparse structures underlying the  $\Sigma_c$  for each component  $c = 1 : 4$ . Figure 6 shows heat maps of approximate posterior

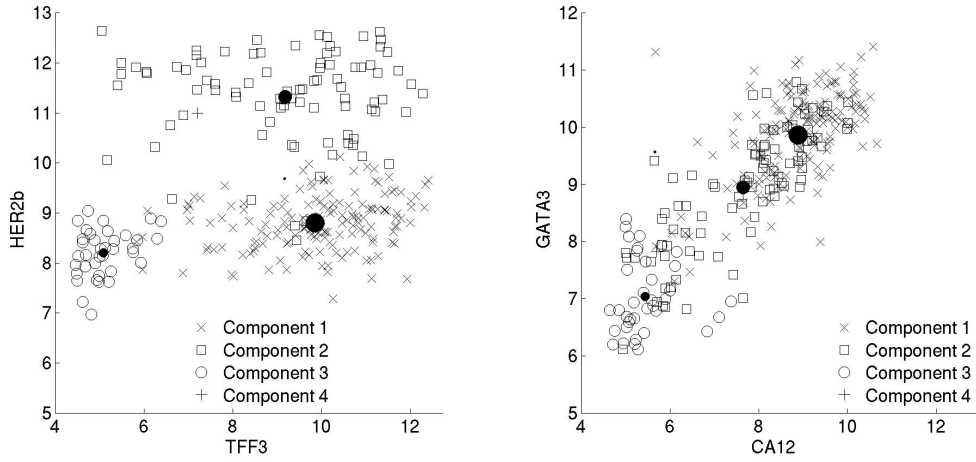


Figure 5: Aspects of estimated component classification summaries in the analysis of the mixture model for the gene expression data. The filled circles correspond to the estimated means of the mixture components and their sizes are proportional to the estimated component weights.

	% non-zero rotators			% zeros in $\mathbf{R}$		
	2.5%	50%	97.5%	2.5%	50%	97.5%
Component 1	9.5	10.5	12.1	66.8	71.8	73.7
Component 2	8.4	10.0	11.0	74.5	82.6	87.4
Component 3	1.6	3.2	4.2	95.3	92.1	97.6

Table 1: Posterior medians and end-points of approximate posterior 95% credible intervals for the percentage of sparse elements of  $\mathbf{R}_c$  and of the number of rotators in each of the mixture components  $c = 1, 2, 3$ .

probabilities of non-zero values in the precision matrices  $K_c = \Sigma_c^{-1}$  indicating the nature of sparsity and the underlying graphical model structure. Component  $c = 1$  has high probabilities on multiple edges linking pairs of ER related genes, Her2 related genes and tying in the two BRCA genes. Component  $c = 2$  more sharply identifies a Her2-related cluster and a distinct ER-related cluster, with somewhat weaker links to the two related BRCA genes. The much sparser component  $c = 3$  highlights links only between Her2 related genes.

Finally, we see that, appropriately, the low probability component  $c = 4$  has really no structure at all, consistent with prior for a basically empty component. These conditional dependencies, and independencies, are better understood in terms of the estimated factor structure underlying eigenmatrices and eigenvalues of the sparse Givens models in each component; these are shown in the left column of Figure 7 for the three main components. For the “high ER” tumors in component  $c = 1$ , we see one dominant and two subsidiary eigenvectors, indicating three “ER-related factors” based on non-zero loadings of the ER-related genes; these presumably reflect several dimensions of the underlying patterns of variability in these genes as a result of the complexity of the ER network. The second dominant

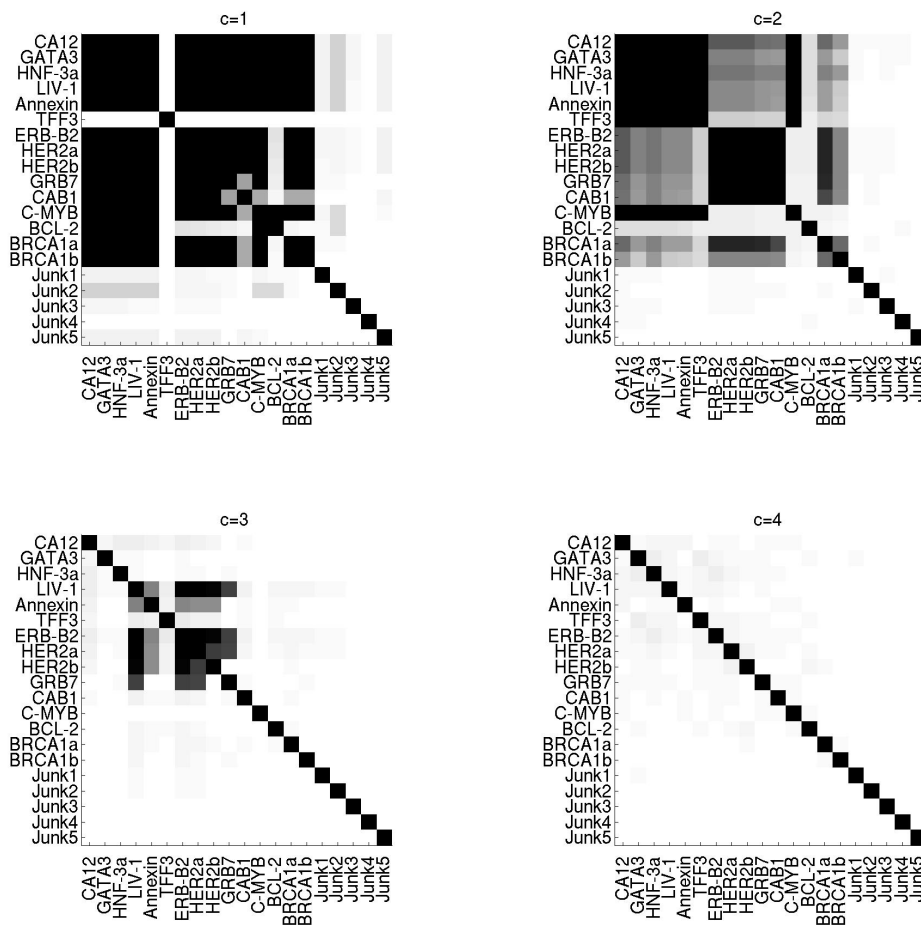


Figure 6: Heat maps showing posterior probabilities of non-zero entries in  $K_c$  for each normal mixture component  $c = 1 : 4$  in analysis of cancer gene expression data. Shading runs from white=0 to black=1 in each.

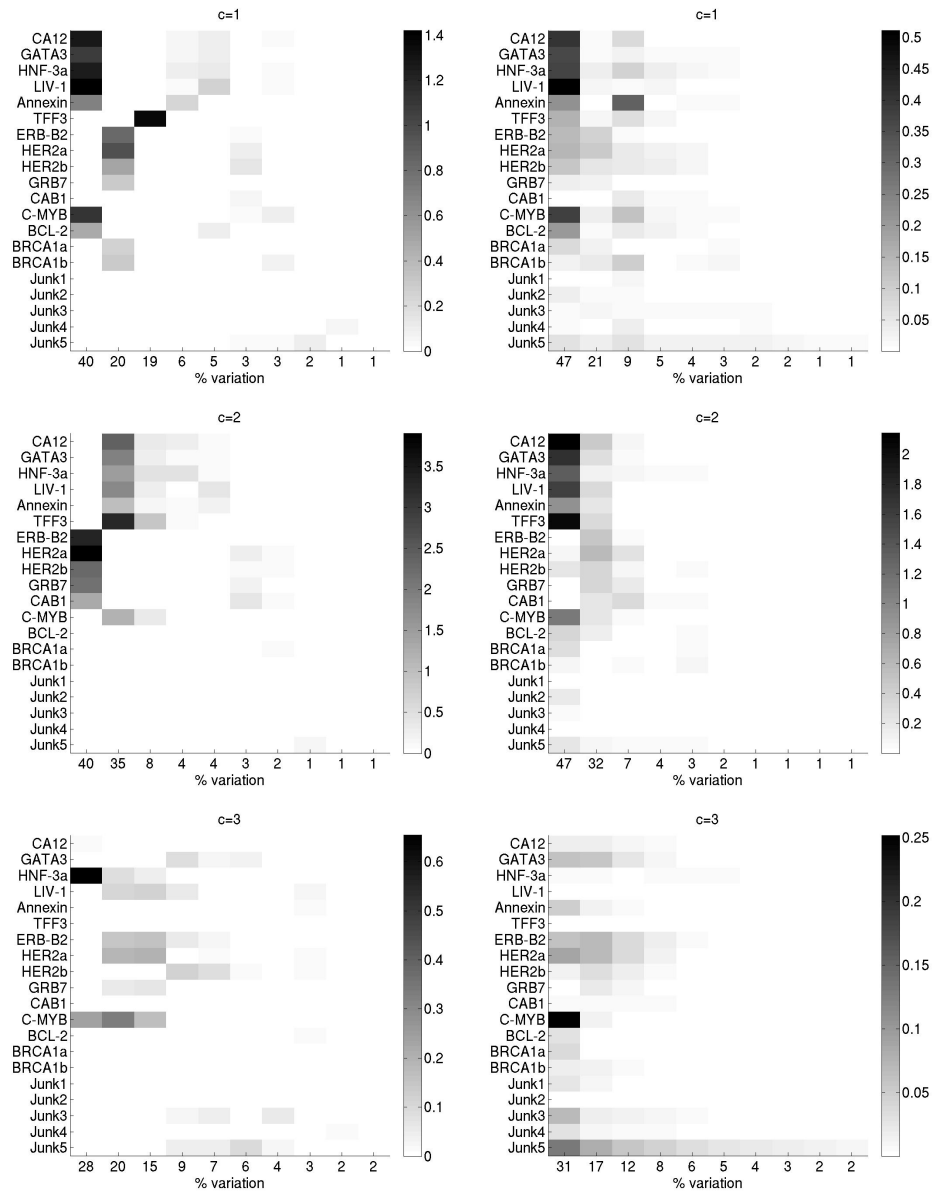


Figure 7: Heat maps showing posterior means of the first 10 columns of  $R_c D_c^{1/2}$  for the three main mixture components in analysis of cancer gene expression data. Left column: Sparsity model, and Right column: full non-sparse model. The percent variation explained by each eigenvector is indicated on the x-axes, based on posterior means of the  $d_j$  in each case.

eigenvector relates to the Her2 cluster. For the “high Her2” tumors in  $c = 2$ , we see the dominant factor is indeed linked to the Her2 gene cluster, while the fact that ER related genes vary across the scale in these tumors leads to a natural set of three or four ER-related factors. For the triple negative/basal-like tumors in component  $c = 3$ , we see residual biological pathway activity highlighted involving HNF-3 $\alpha$  and C-MYB genes, as well as important factors in both ER and Her2 pathways; although these two pathways are less active in tumors in this group, there is still meaningful variation among subsets of some of these genes.

For comparison, the right column in Figure 7 shows the corresponding eigenstructure extracted from an analysis using traditional inverse Wishart priors on the  $\Sigma_c$ , i.e., in the standard analysis with no sparsity. It is very clear how the sharp factor-based groupings in the sparse Givens mixture model “cleans-up” the much noisier standard results. In addition to cleaner and focused inference on dependency structures, we also found that the standard analysis— by comparison with the sparse model— generates over-diffuse estimates of the spread of mixture components and so less sharp classification of samples, as a result.

## 8. Additional Comments

In terms of modelling variations and extensions, one interesting question relates to the interpretation of the sparse Givens model as factor analysis. Our examples have stressed this interpretation from an applied viewpoint. Theoretically, the Givens model is a full-rank, orthogonal factor analysis model. We can imagine extensions to include reduced rank approximations that would be based on the use of priors giving positive probability to zero values among the  $d_i$ , relating more directly to alternative factor modelling frameworks [39].

We have experience in running the MCMC analysis for higher-dimensional variance matrices, including extensions of the gene expression examples with  $q = 300$  genes. The overall performance of the MCMC is scalable, in terms of acceptance rates, while of course the running time and implementation overheads increase. In particular, as the number of rotators grows, a number of computational challenges arise. First, the numerical optimization to define Metropolis proposals  $g_c(\omega_{i,j})$  becomes increasingly time consuming, so that one immediate area of research will be to explore more computationally efficient proposal strategies for the MCMC. Second, based on our positive experience with the exploratory analysis to define ad-hoc starting values for increasingly high-dimensional problems, one direction for improving the MCMC would be to consider alternatives to the birth/death strategy based on more aggressive local search in neighborhoods of “good” sparsity configurations. Some of the concepts and computational strategies underlying shotgun stochastic search in regression and graphical models [19, 16, 14, 15] may be of real benefit here. The potential for distributed computation, including using GPU hardware [34, 35, 13] is also of interest.

### Supplementary Material

As noted in the text, code implementing the analyses reported here is (freely) available to interested readers at the authors’ web site.

## Appendix: MCMC in Mixtures of Sparse Givens Models

Additional technical details of the MCMC algorithm in Section 7 are given here.

(a) *Starting values*: We use  $k$ -means clustering to define initial, crude classification of the data into  $C$  groups, giving starting values for component indicators  $\gamma$ . Group means and proportions define starting values  $\boldsymbol{\mu}_c$  and  $w_c$ . Initial values for the Givens structures within each group are then created using the exploratory algorithm of Section 4. Beginning with the sample variance matrix of each group  $c$ , this algorithm produces a sparse Givens structure with starting values for the rotator pairs, angles and eigenvalues, and hence  $\mathbf{R}_c$ ,  $\mathbf{D}_c$  and  $\boldsymbol{\Sigma}_c$ . The measurement error variances  $\psi_j$  in  $\boldsymbol{\Psi}$  are initialized at draws from the prior.

(b) *Rotator structure and angle updates*: For each cluster  $c = 1 : C$  defined at the current iterate of the MCMC, we update the rotators selected and corresponding angles using the RJ-MCMC analysis of Section 5.3.

(c) *Latent data  $\mathbf{X}$* : Each  $\mathbf{x}_i$  is resampled from the complete conditional normal posterior whose mean vector  $\mathbf{m}_i$  and variance matrix  $\mathbf{M}_i$  are given by

$$\mathbf{m}_i = \mathbf{M}_i(\boldsymbol{\Psi}^{-1}\mathbf{y}_i + \boldsymbol{\Sigma}_{\gamma_i}^{-1}\boldsymbol{\mu}_{\gamma_i}) \quad \text{and} \quad \mathbf{M}_i^{-1} = \boldsymbol{\Psi}^{-1} + \boldsymbol{\Sigma}_{\gamma_i}^{-1}.$$

Note that the  $\boldsymbol{\Sigma}_c^{-1}$  can be calculated trivially even in high dimensional cases simply by inverting the eigenvalues.

(d) *Measurement error variances  $\psi_j$* : Each of the  $q$  elements of the diagonal matrix  $\boldsymbol{\Psi}$  is resampled from a complete conditional given by

$$\psi_j^{-1} \sim Ga(\phi_a + n/2, \phi_b + \sum_{i=1}^n \epsilon_{ji}^2/2)$$

for  $j = 1 : q$ , where  $\epsilon_{ji}$  is the  $j$ -the element of  $\mathbf{y}_i - \mathbf{x}_i$ .

(e) *Component indicators  $\gamma$* : The set of  $n$  component classification indicators  $\boldsymbol{\gamma} = (\gamma_1, \dots, \gamma_n)'$  are drawn from conditionally independent multinomials, each with sample size 1 and probabilities over the  $C$  cells defined by

$$Pr(\gamma_i = c | \cdot) \propto w_c N(\mathbf{x}_i | \boldsymbol{\mu}_c, \boldsymbol{\Sigma}_c), \quad c = 1 : C,$$

where  $N(\mathbf{x} | \cdot, \cdot)$  denotes the multivariate normal pdf.

(f) *Component weights  $w$* : Resampled weights come from the complete conditional Dirichlet posterior with parameter  $(\alpha_1, \dots, \alpha_C)'$  and  $\alpha_c = 1/C + n_c$  where

$$n_c = \sum_{i=1}^n I(\gamma_i = c), \quad c = 1 : C.$$

(g) *Component means  $\boldsymbol{\mu}_c$* : Denote by  $\bar{\mathbf{x}}_c$  the sample mean in group  $c$  given a current set of component indicators. Then the component means are sampled in parallel from the  $C$  conditional normal posteriors with means  $(n_c + 1/\tau)^{-1}n_c\bar{\mathbf{x}}_c$  and variance matrices  $(n_c + 1/\tau)^{-1}\boldsymbol{\Sigma}_c$ ,  $c = 1 : C$ .

(h) *Eigenvectors  $\mathbf{D}_c$* : Finally, the complete conditional distributions of the diagonal elements of  $\mathbf{D}_c = \mathbf{A}_c^{-1}$  are independent inverse gammas constrained by the ordering; see (12), applied to each of the  $C$  groups in parallel. These are sampled in sequence using the inverse cdf method.

## References

- [1] T. W. Anderson, I. Olkin, and L. G. Underhill. Generation of random orthogonal matrices. *SIAM Journal on Scientific and Statistical Computing*, 8:625–629, 1987. [2](#), [3](#), [9](#)
- [2] C. M. Carvalho, J. E. Lucas, Q. Wang, J. Chang, J. R. Nevins, and M. West. High-dimensional sparse factor modelling - Applications in gene expression genomics. *Journal of the American Statistical Association*, 103:1438–1456, 2008. [2](#), [9](#), [15](#), [17](#)
- [3] C. M. Carvalho and M. West. Dynamic matrix-variate graphical models. *Bayesian Analysis*, 2:69–98, 2007. [4](#), [14](#)
- [4] C. Chan, F. Feng, J. Ottinger, D. Foster, M. West, and T. B. Kepler. Statistical mixture modelling for cell subtype identification in flow cytometry. *Cytometry, A*, 73:693–701, 2008. [15](#)
- [5] Andrew J. Cron and Mike West. Efficient classification-based relabeling in mixture models. *The American Statistician*, 65:16–20, 2011. [16](#)
- [6] M.J. Daniels and M. Pourahmadi. Modeling covariance matrices via partial autocorrelations. *Journal of Multivariate Analysis*, 100:2352–2363, 2009. [2](#)
- [7] A. Dobra, B. Jones, C. Hans, J. R. Nevins, and M. West. Sparse graphical models for exploring gene expression data. *Journal of Multivariate Analysis*, 90:196–212, 2004. [4](#), [14](#)
- [8] A. Dobra, A. Lenkoski, and A. Rodriguez. Bayesian inference for general Gaussian graphical models with application to multivariate lattice data. *Journal of the American Statistical Association*, 106:1418–1433, 2012. [2](#), [4](#), [14](#)
- [9] M. D. Escobar and M. West. Bayesian density estimation and inference using mixtures. *Journal of the American Statistical Association*, 90:577–588, 1995. [15](#)
- [10] N. I. Fisher. *Statistical Analysis of Circular Data*. Cambridge University Press, 1993. [12](#)
- [11] D. R. Fulkerson and O. A. Gross. Incidence matrices and interval graphs. *Pacific Journal of Mathematics*, 15:835–855, 1965. [5](#)
- [12] Peter J. Green. Reversible jump Markov chain Monte Carlo computation and Bayesian model determination. *Biometrika*, 82:711–732, 1995. [12](#)
- [13] L. F. Gruber and M. West. GPU-accelerated Bayesian learning in simultaneous graphical dynamic linear models. *Bayesian Analysis*, - Advance Publication, 2 March 2015:<http://projecteuclid.org/euclid.ba/1425304898>, 2015. [2](#), [21](#)
- [14] C. Hans, A. Dobra, and M. West. Shotgun stochastic search in regression with many predictors. *Journal of the American Statistical Society*, 102:507–516, 2007. [21](#)
- [15] C. Hans, Q. Wang, A. Dobra, and M. West. SSS: High-dimensional Bayesian regression model search. *Bulletin of the International Society for Bayesian Analysis*, 24:8–9, 2007. [21](#)
- [16] C. Hans and M. West. High-dimensional regression in cancer genomics. *Bulletin of the International Society for Bayesian Analysis*, 13:2–3, 2006. [21](#)

- [17] Peter D. Hoff. Simulation of the matrix Bingham-von Mises-Fisher distribution, with applications to multivariate and relational data. *Journal of Computational and Graphical Statistics*, 18:438–456, 2009. [8](#)
- [18] E. S. Huang, M. West, and J. R. Nevins. Gene expression profiles and predicting clinical characteristics of breast cancer. *Hormone Research*, 58:55–73, 2002. [9](#)
- [19] B. Jones, A. Dobra, C. M. Carvalho, C. Hans, C. Carter, and M. West. Experiments in stochastic computation for high-dimensional graphical models. *Statistical Science*, 20:388–400, 2005. [21](#)
- [20] B. Jones and M. West. Covariance decomposition in undirected Gaussian graphical models. *Biometrika*, 92:779–786, 2005. [2](#), [4](#), [14](#)
- [21] S. L. Lauritzen. *Graphical Models*. Clarendon Press, Oxford, 1996. [4](#), [14](#)
- [22] M. Lavine and M. West. A Bayesian method for classification and discrimination. *Canadian Journal of Statistics*, 20:451–461, 1992. [16](#)
- [23] H. F. Lopes, R. E. McCulloch, and R. Tsay. Cholesky stochastic volatility. Technical report, University of Chicago, Booth Business School, 2010. [2](#)
- [24] J. E. Lucas, C. M. Carvalho, J. T. A. Chi, and M. West. Cross-study projections of genomic biomarkers: An evaluation in cancer genomics. *PLoS One*, 4:e4523, 2009. [15](#), [17](#)
- [25] J. E. Lucas, C. M. Carvalho, D. Merl, and M. West. In-vitro to In-vivo factor profiling in expression genomics. In D. Dey, S. Ghosh, and B. Mallick, editors, *Bayesian Modelling in Bioinformatics*, pages p293–316. Taylor-Francis, 2010. [15](#), [17](#)
- [26] J. E. Lucas, C. M. Carvalho, Q. Wang, A. H. Bild, J. R. Nevins, and M. West. Sparse statistical modelling in gene expression genomics. In K.A. Do, P. Mueller, and M. Vannucci, editors, *Bayesian Inference for Gene Expression and Proteomics*, pages 155–176. Cambridge University Press, 2006. [15](#), [17](#)
- [27] J. E. Lucas, C. M. Carvalho, and M. West. A Bayesian analysis strategy for cross-study translation of gene expression biomarkers. *Statistical Applications in Genetics and Molecular Biology*, 8:Article 11, 2009. [9](#), [15](#), [17](#)
- [28] G.J. McLachlan, D. Peel, and R.W. Bean. Modelling high-dimensional data by mixtures of factor analyzers. *Computational Statistics and Data Analysis*, 41:379–388, 2003. [16](#)
- [29] J. Nakajima and M. West. Bayesian analysis of latent threshold dynamic models. *Journal of Business & Economic Statistics*, 31:151–164, 2013. [2](#)
- [30] A. Rodriguez, A. Lenkoski, and A. Dobra. Sparse covariance estimation in heterogeneous samples. *Electronic Journal of Statistics*, 5:981–1014, 2011. [2](#), [4](#), [14](#), [16](#)
- [31] D. M. Seo, P. J. Goldschmidt-Clermont, and M. West. Of mice and men: Sparse statistical modelling in cardiovascular genomics. *Annals of Applied Statistics*, 1:152–178, 2007. [17](#)
- [32] D. M. Seo, T. Wang, H. K. Dressman, E. E. Herderick, E. S. Iversen, C. Dong, K. Vata, C. A. Milano, F. Rigat, J. Pittman, J. R. Nevins, M. West, and P. J. Goldschmidt-Clermont. Gene expression phenotypes of atherosclerosis. *Arteriosclerosis, Thrombosis and Vascular Biology*, 24:1922–1927, 2004. [17](#)

- [33] T. Sørli. Molecular portraits of breast cancer: Tumour subtypes as distinct disease entities. *European Journal of Cancer*, 40:2667–75, 2004. [9](#), [15](#), [17](#)
- [34] M. A. Suchard, C. Holmes, and M. West. Some of the *What?*, *Why?*, *How?*, *Who?* and *Where?* of graphics processing unit computing for Bayesian analysis. *Bulletin of the International Society for Bayesian Analysis*, 17:12–16, 2010. [21](#)
- [35] Marc A. Suchard, Quanli Wang, Cliburn Chan, Jacob Frelinger, Andrew Cron, and Mike West. Understanding GPU programming for statistical computation: Studies in massively parallel massive mixtures. *Journal of Computational and Graphical Statistics*, 19:419–438, 2010. [15](#), [21](#)
- [36] M. West. Bayesian factor regression models in the “large p, small n” paradigm. In J. M. Bernardo, M. J. Bayarri, J. O. Berger, A. P. David, D. Heckerman, A. F. M. Smith, and M. West, editors, *Bayesian Statistics 7*, pages 723–732. Oxford University Press, 2003. [2](#)
- [37] M. West, C. Blanchette, H. K. Dressman, E. S. Huang, S. Ishida, H. Zuzan R. Spang, J. R. Marks, and J. R. Nevins. Predicting the clinical status of human breast cancer utilizing gene expression profiles. *Proceedings of the National Academy of Sciences*, 98:11462–11467, 2001. [9](#)
- [38] R. Yang and J. O. Berger. Estimation of a covariance matrix using the reference prior. *Annals of Statistics*, 22:1195–1211, 1994. [3](#)
- [39] R. Yoshida and M. West. Bayesian learning in sparse graphical factor models via annealed entropy. *Journal of Machine Learning Research*, 11:1771–1798, 2010. [2](#), [21](#)